# Brain MRI tumor detection using Deep learning Techniques

**Katam Naga Lakshman[1], Dr. Amit Singal[2], Dr. A. Ramaswami Reddy[3]**

[1]Research Scholar, Computer Science and Engineering, Monad University, N.H.09, Delhi - Hapur Road, P.O Pilkhuwa, Distt. Hapur - 245304, (U.P), [2]Professor, Department of Computer Science and Engineering, Monad University Hapur, (U.P.) India, [3]Professor, Computer Science and Engineering, Malla Reddy Engineering College, Maisammaguda, Secunderabad, India

**Abstract:** All age groups have a high incidence of brain tumours, hence early and precise diagnosis of tumour type is essential for selecting the most effective treatment plan(s). Neuroradiologists have been able to identify brain tumours more reliably using convolutional neural networks (CNNs) by using magnetic resonance imaging (MRIs). If the number of MRIs in the system is too low, CNN's learning suffers from overfitting. The augmentation approach is currently the best answer to this issue, since it optimises the learning stage and hence enhances the total efficiency. New methods for analysing brain tumour MRIs will be tested in this project using a VGG19 features extractor paired with one or more of three different classifiers. Neuroimaging of brain tumours may be improved by using a PGGAN (progressive growing generative adversarial network) augmentation model, which produces'realistic' MRIs. A precision of 98.54 percent was found in the classification of gliomas, meningiomas, and pituitary tumours using our framework. We also looked at a variety of other performance indicators.

**Keywords:** Brain tumor detection, CNN, Deep learning

## 1. Introduction:

Cancer is one of the most common causes of death in the globe. Cancer is a disease that may affect any region of the body and is very difficult to treat. Because of the vast range in severity, length, location, and chemotherapeutic treatment sensitivity/resistance, it's possible that tumours aren't being properly classified. Patients with brain tumours have increased significantly over the last decade, making them the 10th most prevalent kind of tumour in both children and adults. It is apparent that a precise categorization of brain tumours would lead to more efficient medical treatment and a better prognosis for the patients. Neuro-oncologists have benefited from CAD approaches in a variety of ways. Early diagnosis and categorization of brain cancers have been helped by CAD approaches [2]. Physicians who use computer-aided diagnosis (CAD) are better able to classify patients than those who depend only on visual comparisons [3]. It is possible to get a wealth of information about brain tumours using magnetic resonance imaging (MRI), which does not need the use of dangerous ionising radiation. MRIs are superior than CT scans when it comes to detecting soft tissues. When used in conjunction with computer-aided design

(CAD), MRIs may assist swiftly pinpoint tumour locations and sizes [5,6]. Because of technological advancements, doctors may now use more precise diagnostic tools. There has been a notable improvement in medical image analysis and treatment-related decision making thanks to the advent of deep learning-based systems. This is particularly true when skilled experts employ deep neural networks-based technology. For medical imaging professionals, CAD has become an increasingly popular approach of diagnosis thanks to the fast development of deep learning algorithms and their capacity to better identify medical pictures. One of the highest priorities for radiology researchers right now is expanding research into the use of deep learning to the categorization of different disorders. When it comes to medical picture analysis for various disorders, CNNs are a go-to method among the several deep machine learning (ML) approaches that exist. Such tumors/diseases as lung cancer [10,11], pneumonia [12], colon cancer [13], and liver disease [14] may be accurately classified and predicted using CNNs. It has been utilised to develop a deep learning system for human skin identification as part of dermatological diagnostics, as well as in models of brain tumour detection and segmentation [16,17] and COVID-19 classification without the need for any human intervention. However, although CNNs may be used to help in the categorization of single-label photos, most real-world photographs have several labels with various objects, proprieties and features inside one image. RNNs, unlike other forward neural networks, use multi-label image classification to develop distinct classifiers for each picture attribute. The periodic connections between the nodes in layers are hidden by RNNs, allowing them to categorise serialised input while still capturing dynamic information [18]. RNNs come in a variety of flavours, including BiLSTM and Bidirectional-GRU (Bi-GRU). CNN and RNN (the Gated Recurrent Unit and Long Short-Term Memory networks model) function together to produce models with good illness classification accuracy [19,20]. This has been shown in many research [19, 20]. The absence of a large enough sample size in a data set might hinder the optimum performance of a deep learning model. Several recent studies have attempted to increase the size of their data sets by using data augmentation. CNNs may then examine the data's invariances to produce more robust training models. The issue of overfitting in CNNs may be alleviated by utilising a variety of transformations, including as rotations, flips, and random transformations, to artificially expand the data set [21–23]. In 2014, I. Goodfellow et al. proposed a generative adversarial network (GAN) [24]. New images may be generated from a latent vector by using this deep machine learning algorithm. Basically, it has a generator and a discriminator. To learn how to produce new pictures, the generator model learns to map the latent space to specific locations in the image space. Discriminator models are trained to distinguish between actual and fraudulent pictures. The two models work together to learn how to create convincingly realistic synthetic pictures (such as faces, buildings, and rooms). The GAN model has played a crucial role in addressing the issue of deep learning overfitting as a data augmentation tool. Even if both generator and discriminator of the DCGAN GAN model are implemented using a CNN network, the required resolution of 512 x 512 can't be achieved, as shown in [25]. For example, DCGAN can manufacture X-ray pictures of the chest in order to augment the labelled data set and hence

and synthetic images (DCNNs). These five classifications of chest X-rays allow for the identification of pathology. With DCGAN's capacity to create a realistic set of samples for instructional purposes [8], this method has previously been used effectively to undertake unsupervised training of radiologists. It has also been shown that modified GANs may be used to increase the quality of medical picture data. The WHO classifies brain tumours into four classes (grades I to IV), with grades I and II being categorised as low-grade tumours and grades III and IV being classified as high-grade tumours. Surgery, radiation, chemotherapy, and non-chemotherapeutic drug parameters are all essential in the management of patients with metastatic brain tumours (mTBT) (28). It is one of the most promising areas of deep learning research for medical reasons and is the major foundation for deciding on the primary therapy and the treatment process, as well as estimating the likely success rate of treatment, and mapping out the disease's course of follow-up [29]. Several methods for feature selection and categorization are discussed. The categorization of brain tumours is the primary goal of this study, which includes the following contributions: Multiple brain cancers (gliomas, meningiomas, and pituitary tumours) can be accurately classified by MRIs using three distinct deep learning models. For example, there is VGG19 + CNN (VGG19 + CNN), and VGG19 + GRU (Gated Recurrent Unit) (Bi-GRU). The data set size is increased using two types of data augmentation: conventional data augmentation and PGGAN data augmentation. The models and their applications are compared in detail. The paper also examines Cheng et al. [30]'s shared data collection. Two. Equipment and Methods An MRI will reveal gliomas, meningiomas, and pituitary tumours as three different forms of deadly brain cancer that may be treated with radiation and surgery. The prognosis for these cancers might be bleak if identified late [4].

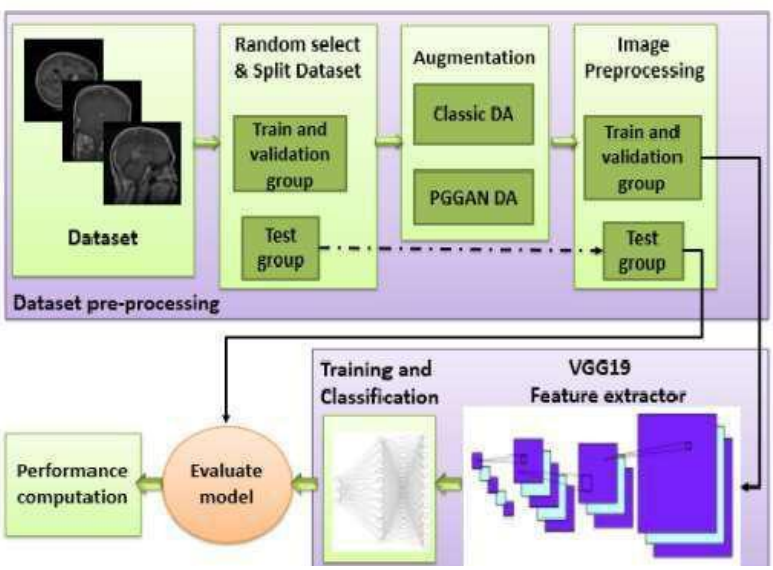


Figure 1: Block diagram of the proposed framework (DA: Data augmentation).

In addition to meningiomas, one of the most prevalent types of primary brain tumours is glioma. The most common intracranial tumours are pituitary adenomas. Their high mortality and morbidity rates [41] are a result of their presence. There is a specific categorization system for each tumour type, and each tumour type has a varied degree of severity, size, and form. Tumor types may be classified based on their distinctions [42]. Brain cancers are better classified with MRIs. An proper diagnosis of a patient's cancer and the development of an effective treatment plan are all dependent on being able to appropriately define the tumour type. Here, the experimental data, their interpretations, and the experimental inferences that may be taken are

framework was created. We used a deep learning model to extract features from the dataset, and then used that model in conjunction with a classification stage (as shown in Figure 1). Brain cancers have been classified using three separate models: VGG19 plus CNN, VGG19 plus GRU, and VGG19 plus Bi-GRU. A radiologist's burden will be reduced and decisions will be made more quickly if this framework can properly diagnose brain cancers.

### 2.1. Data Set for the Study

We utilised Cheng et al. [30]'s open data collection for this study. Deep learning frameworks may be trained and tested using this data set, which was designed to synthesise pictures for training and testing. Gliomas (1426 pictures), meningiomas (708 photos), and pituitary tumours (512 images) comprised the 3064 T1-CE MR images in the data collection, as shown in Figure 2. (930 images). Three planes of MR images were included in the data collection, each having an image size of 512 pixels wide. Figure 3 shows a selection of photos of three tumour kinds from three different planes. Feature extraction and classification are both part of a deep learning model in Stage 4 of 19. Brain cancers have been classified using three separate models: VGG19 plus CNN, VGG19 plus GRU, and VGG19 plus Bi-GRU. Radiologist's effort may be reduced and decision-making more expeditious by appropriately diagnosing brain cancers using this paradigm. Figure 1: Proposed framework block diagram (DA: Data augmentation). 2.1. Research Data Set In this study, we drew on the publicly available data collection created by Cheng et al. [30]. For the training of deep learning frameworks and the assessment of how accurate they are in identifying brain cancers on MRIs, this data set was produced. Gliomas (1426 pictures), meningiomas (708 photos), and pituitary tumours (512 images) comprised the 3064 T1-CE MR images in the dataset (930 images). The MR scans in the data set had a resolution of 512 512 pixels and spanned three planes (axial, sagittal, and coronal). Figure 3 shows a selection of photos of the three tumour types from three different planes.

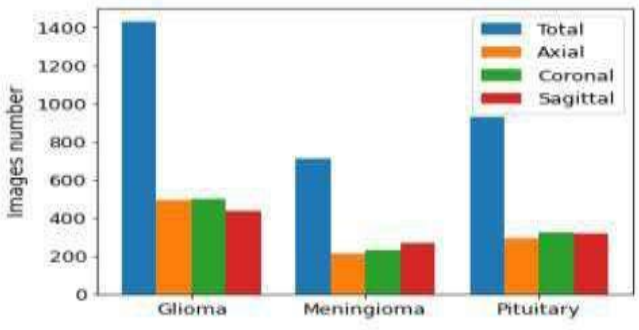

Figure 2. Distribution of each brain tumor type by plane. Distribution of each brain tumor type by plan

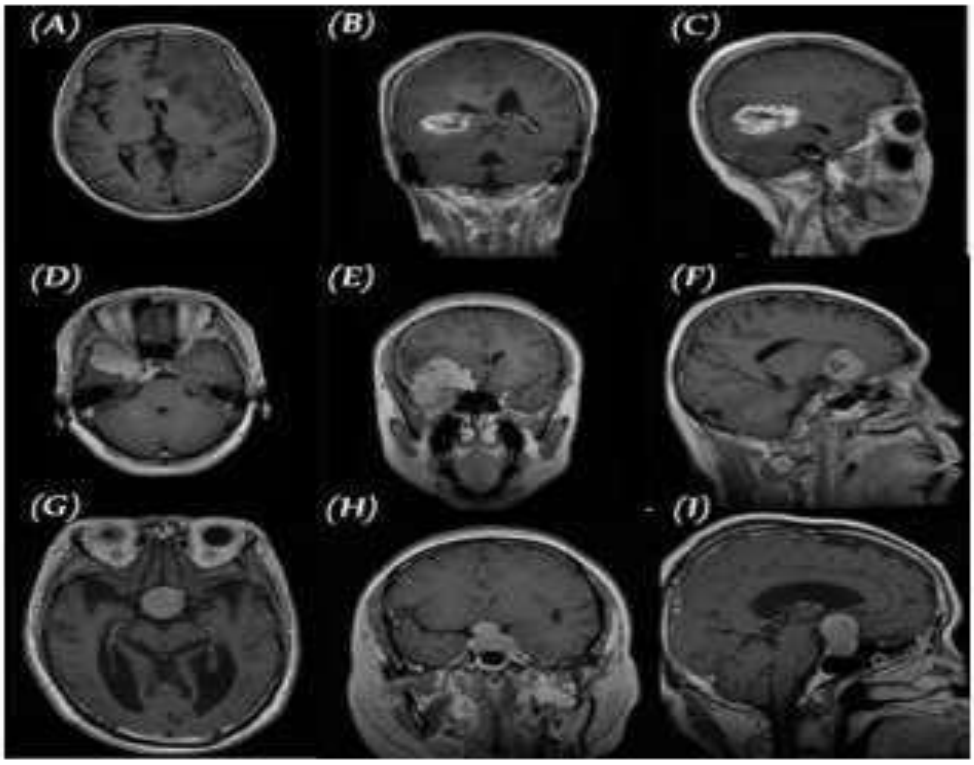


Figure 3. Three planes for three samples of brain tumor MR images from the primary data set, (A–C) glioma, (D–F) meningioma, and (G–I) pituitary.

**2.2. Pre-Processing and Image Augmentation**

Each CNN has hundreds of parameters that need to be taught, even the smallest. To avoid overfitting, CNN models should only be used with large datasets. We used two approaches of data augmentation (DA) to address this issue: conventional augmentation and PGGAN-based augmentation. When using MR pictures, the best results are often achieved without any preprocessing. Because of this, the range of picture intensities has been reduced to For the

purposes of training, validation, and testing, the data set was randomly separated into three groups with the goal label: (15 percent).

### 2.2.1. Classic Data Augmentation

An augmenter was used to expand the amount of the data set in this step. To prevent a model remembering the location of the brain, the brain's position has to be changed sufficiently. For MRIs, the most common DA procedures include the following: In order to ensure that the whole tumour is seen in the final photograph, it is best to rotate the image instead of cropping it. Three rotations were performed: • Mirroring: Images are reflected to the right or left; • Flipping: Images are up or down. As demonstrated in Figure 4, the training and validation groups for the axial, sagittal, and coronal MR images were raised by this strategy.

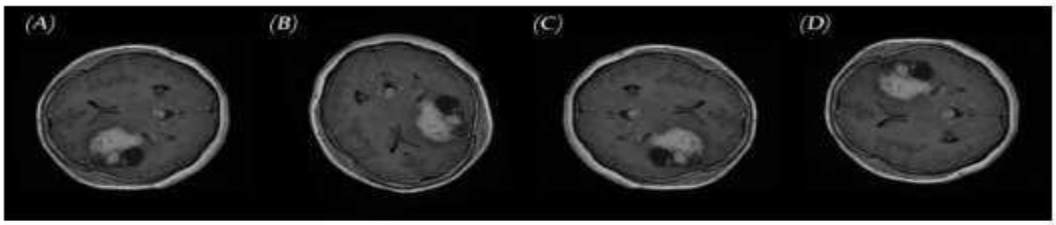


Figure 4. Samples of brain tumor MRIs and results of augmentation: (A) primary MRI, (B) rotation, (C) left-right mirroring, and (D) up–down flipping.

### 2.2.2. PGGAN-Based Data Augmentation

In order to address the imbalance in medical data sets, this study looked at the idea of applying the GAN methodology as an additional way of augmentation. GAN model PGGAN [43] is based on a generator and discriminator that increases over time. With its 1024-by-1024-pixel resolution, it's ideal for training steadiness. In order to overcome a paucity of pictures in the data set, we utilised PGGAN to synthesise brain tumour MRIs in three different planes (axial, sagittal, and coronal). A 512 latent vector was used to create pictures from low-resolution 4 4 pixel photos. Images had a resolution of 256 256 pixels, with the resolution rising by a factor of 2 with each subsequent stage (Figure 5). Each picture in the dataset was used to train the model and create each dimension in a class image [30]. An image-generating neural network (GAN) model, Diagnostics 2021, 11,x FOR PEER REVIEW [43], is capable of synthesising pictures of up to 1024 by 1024 pixels in resolution. For three tumours with the same structure, we utilised PGGAN to fill in the gaps left by the absence of pictures in the data setup for brain tumour MRIs. Latent vectors were used to create images that were four pixels wide and four pixels high. Image resolution increased by a factor of 2 as it progressed from 256x256 to 256x256 (Figure 5). We used the data set's major pictures to train the model and create mensions for each class image [30]. Details of PGGAN implementation: In [43], the original PGGAN was utilised. In order to synthesise MRIs of brain tumours, we trained the model using this PGGAN. If possible, a latent vector of at least 512 should be used to assist high-resolution MRI imaging. There were two

models in the PGGAN architecture utilised to synthesise the brain tumour: the generator and the discriminator. In order to avoid surpassing the system's memory capacity, the batch size was varied during training as follows: 4128, 8128, 16128, 3264, 6432, 12816, and 2564. [44] The Adam optimizer (with a learning rate of 0.001) was selected since it provides the greatest accuracy. A WGAN-GP loss function was utilised [45]. Pixel-wise feature vector normalisation was implemented after each convolution layer, except for the final output layer, as in the work by [21]. In order to activate the layer, the Leaky ReLU has a leakiness of 0.2. It served as a source and a filter at the same time. 2.3. Deep Learning Models Under Consideration Tumors of the pituitary gland, as well as gliomas and meningiomas, may affect the brain.

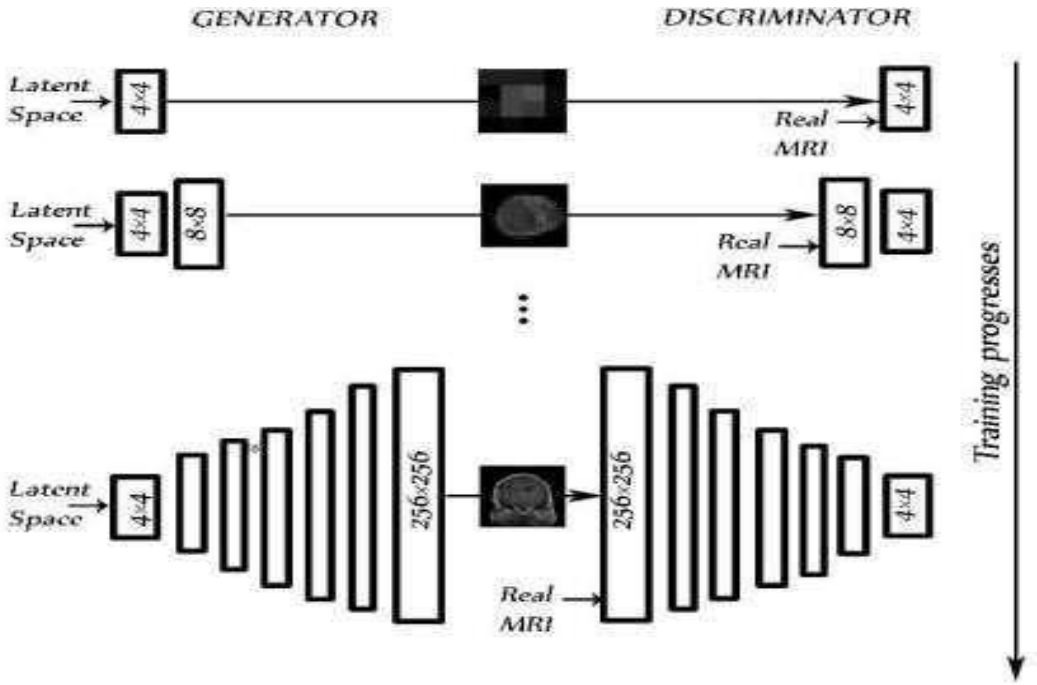


Figure 5. PGGAN architecture for the 256 × 256 pixel MR image brain tumor generator during training progress.

The best way to diagnose and characterise these tumours radiologically is using MRIs. The categorization of MRIs of brain tumours has been improved because to the use of deep machine learning. We wanted to create an intelligent system that could better categorise the MRI images of these three classes, pituitary tumours, and gliomas than the present models. To begin, a VGG19 was utilised to extract features. For large-scale picture applications, VGG19 [46] is a commonly used CNN architectural model consisting of 19 layers, each having 3 x 3 convolution filters, and a stride of 1. Using a VGG19 as a high-accuracy feature extractor was critical to our architecture. Several deep learning classifiers were merged into the VGG19 extractor to achieve the highest level of accuracy in the diagnosis of brain tumours. Classifiers such as VGG19 + CNN and VGG19 + GRU and Bi-GRU were compared to three distinct architectures in order to determine the optimal VGG19 + classifier combination. It was a matter of comparing their performances and selecting the best. As a final step, we compared the same three models to ones that were either enhanced classically or using PGGAN as the basis for the enhancement (augmenters are designed to produce more realistic MRIs). Pre-processing: The input picture was 224 by 224 pixels in size. All MRIs in the dataset were scaled to the same dimensions. PGGAN

created pictures with a resolution of 256 by 256 pixels. In this way, the photos were downsized to a resolution of 244x244 pixels. How to have your data augmented (DA)? The following two DA setups were utilised to evaluate the performance of our models, with enough pictures for each of the three tumour classes: 2.3.1. There are two types of DA: classic and classic plus PGGAN-based. Deep Learning using VGG19 and CNN Brain cancers on MRIs were to be classified using a VGG19 + CNN model, followed by CNN. In this case, features were extracted and classifiers were applied. VGG19 and CNN were employed as feature extraction models in this model. VGG19 + CNN has a total of 139,581,379 trainable parameters, of which 139,581,379 were trainable. Table 2 shows the model's structure; the input layer comprised 224 224 1 MRIs of brain tumours. Each block included a convolution layer with 4096 neurons, followed by a dropout layer with a dropout rate of 0.5, a ReLU activation function, and lastly a SoftMax layer, which classified the output into one of three categories of tumours based on the VGG19 feature extraction.

Table 2. Architecture details of the VGG19+CNN model. The maxpooling layer is applied after each convolution layer.

| VGG19 + CNN Model | Output Shapes |
|---|---|
| [Conv (3 × 3) − 64] × 2 | 224 × 224 × 64 |
| [Conv (3 × 3) − 128] × 2 | 112 × 112 × 128 |
| [Conv (3 × 3) − 256] × 4 | 56 × 56 × 256 |
| [Conv (3 × 3) − 512] × 4 | 28 × 28 × 512 |
| [Conv (3 × 3) − 512] × 4 | 14 × 14 × 512 |
| Max pool | 7 × 7 × 512 |
| Flatten | 25,088 |
| Dense (relu) | 4096 |
| Dropout (0.5) | 4096 |
| Dense (relu) | 4096 |
| Dropout (0.5) | 4096 |
| Dense (SoftMax) | 3 |

### 2.3.2. VGG19 and GRU Deep Learning Model

GRU is an RNN architecture with a number of advantageous features, such as its simplicity and need for less training time, in addition to its ability to store information irrelevant to the predictions made for extended periods of time. Our second deep model,which consisted of a VGG19 model followed by GRU, was designed to classify the MRIs of brain tumors. It employed feature extraction and classification. To our second model, we added GRU as a classifier after VGG19 having been used as feature extraction. Beyond the layers of the VGG19, the output passed to a reshape layer followed by a GRU layer with 512 units, then two blocks consisting of a convolution layer of 1024 neurons followed by a dropout layer, and finally a SoftMax layer, as shown in Table 3 (27,895,747 total parameters).

Table 3. Architecture details of the VGG19 + GRU model.

| VGG19 + GRU Model | Output Shapes |
|---|---|
| [Conv (3 × 3) − 64] × 2 | 224 × 224 × 64 |
| [Conv (3 × 3) − 128] × 2 | 112 × 112 × 128 |
| [Conv (3 × 3) − 256] × 4 | 56 × 56 × 256 |
| [Conv (3 × 3) − 512] × 4 | 28 × 28 × 512 |
| [Conv (3 × 3) − 512] × 4 | 14 × 14 × 512 |
| Max pool | 7 × 7 × 512 |
| Reshape | 7 × 7 × 512 |
| Time Distributed | 7 × 3584 |
| GRU (512) | 512 |
| Dense (relu) | 1024 |
| Dropout (0.5) | 1024 |
| Dense (relu) | 1024 |
| Dropout (0.5) | 1024 |
| Dense (SoftMax) | 3 |

### 2.3.3. VGG19 and GRU Bidirectional Deep Learning Model

We then employed a VGG19 and a Bi-GRU as feature extraction models and classifiers in our final model. Reshaping and Bi-GRU layers were followed by a dropout and dense layer with a SoftMax activation function. The model was composed of six layers. Table 4 depicts the model's structure (34,714,563 total parameters)

Table 4. Architecture details of the VGG19 + Bi-GRU model

| VGG19 + Bi-GRU Model | Output Shapes |
|---|---|
| [Conv (3 × 3) − 64] × 2 | 224 × 224 × 64 |
| [Conv (3 × 3) − 128] × 2 | 112 × 112 × 128 |
| [Conv (3 × 3) − 256] × 4 | 56 × 56 × 256 |
| [Conv (3 × 3) − 512] × 4 | 28 × 28 × 512 |
| [Conv (3 × 3) − 512] × 4 | 14 × 14 × 512 |
| Max pool | 7 × 7 × 512 |
| Reshape | 7 × 7 × 512 |
| Time Distributed | 7 × 3584 |
| Bidirectional | 1024 |
| Dense (relu) | 1024 |
| Dropout (0.5) | 1024 |
| Dense (relu) | 1024 |
| Dropout (0.5) | 1024 |
| Dense (SoftMax) | 3 |

VGG19 + GRU was proven to have a lesser number of parameters than the other models in Figure 6 when compared to other models. Because of this, it was the simplest. An extensive set of parameters went into the development of the VGG19 + CNN model.

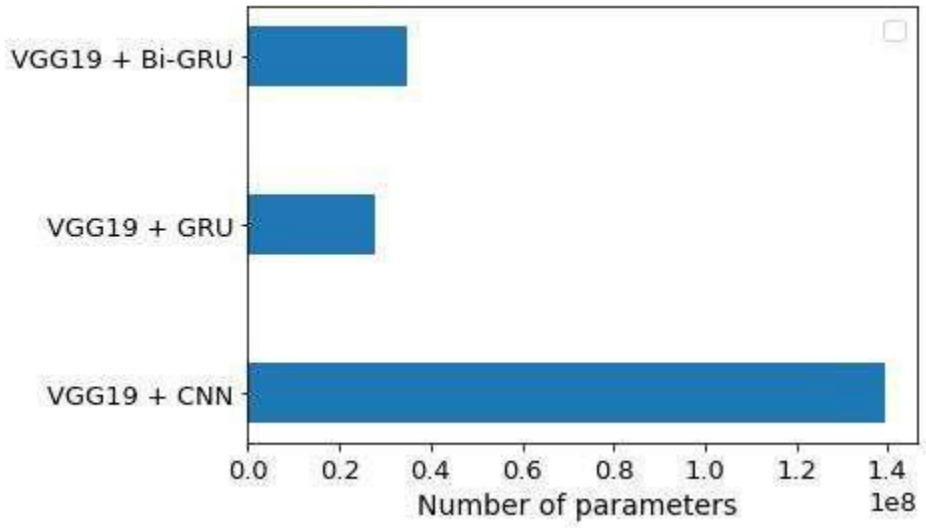


Figure 6. Number of trainable parameter-wise distributions for each of the three models.

## 3. Results

TensorFlow and Keras frameworks were used to train all classification models in the framework constructed for this research, using the following specification: 2 TB of storage, 12 GB of RAM, and at least a P100 GPU are required. In order to choose the optimum hyperparameters for the final model assessment, we ran a series of experiments. With a batch size of 32 and a categorical cross-entropy loss for multi-classification, we trained our model for 100 epochs without pre-training on ImageNet. We examined the accuracy of the [44], RMSprop [47], or Nadam [48] for the three models to determine the optimal optimizer. When we evaluated the models using these four optimizers, we found that the models were accurate. Our learning rate was set at 0.00001.

### 3.1. Performance Metrics

For the purpose of classifying links between data and distributions, recent research have employed confusion matrices to study models and measure the performance level of the classification process. Various confusion matrices may be used to test classification models extensively [49]. Tests on the classifier employed four major keys: Tp, Tn, Fp, and Fn, which stand for true positive and false negative, respectively. The model's accuracy (ACC), sensitivity (SPC), specificity (SPC), precision (PPV), negative predictive values (NPVs), the F1-score, and Matthew's correlation coefficient were calculated based on the four outcomes (MCC).

### 3.2. Scenario I: Deep Learning Models with Classic Augmentation

Increase the picture count to get a more comprehensive design for brain tumour categorization in all three dimensions. All three planes were boosted using a traditional augmenter. The Nadam optimizer was used for the VGG19 + CNN model, as shown in Table 5, to reach the greatest accuracy of 96.59 percent. VGG19 + CNN model's additional performance metrics for the three

kinds of brain tumours are included in Table 6. It was pituitary tumours that accounted for the best results. Glioma detection was obtained with the best sensitivity and the highest NPV values by the model.

**Table 5.** Comparison between different optimizers for the three proposed models.

| Models | Adam | Adamax | RMSprop | Nadam |
|---|---|---|---|---|
| VGG19 + CNN | 94.16 | 92.94 | 95.59 | **96.59** |
| VGG19 + GRU | **94.89** | 87.10 | 93.19 | 93.67 |
| VGG19 + BI-GRU | 95.38 | 89.05 | **95.62** | 92.94 |

The bold values indicate the best accuracy value that was achieved.

Gliomas, meningiomas, and pituitary tumours were all correctly recognised by our VGG19 + CNN model in 90.2 percent of instances, whereas pituitary tumours were correctly detected in 96.92 percent of cases. We classified brain cancers in MRIs using a mix of CNN and RNN models. VGG19 and GRU models were merged in order to analyse the picture properties and learn the structural aspects of tumours.



Table 6. All performance results for the three proposed models (where Men, Gli, and Pit refer to meningioma, glioma, and pituitary tumor, respectively).

| Model | Class | Accuracy | Precision | Sensitivity | F1-Score | Specificity | NPV | MCC |
|---|---|---|---|---|---|---|---|---|
| VGG19 + CNN | Gli. | 96.97 | 93.81 | 100 | 96.81 | 94.56 | 100 | 94.10 |
| | Men. | 97.44 | 98.92 | 90.2 | 94.56 | 99.70 | 97.02 | 92.87 |
| | Pit. | 99.06 | 100 | 96.92 | 98.44 | 100 | 98.68 | 97.83 |
| VGG19 + GRU | Gli. | 95.01 | 95.87 | 89.52 | 92.8 | 97.84 | 94.58 | 89.01 |
| | Men. | 94.46 | 87.77 | 94.12 | 90.1 | 94.96 | 97.61 | 86.78 |
| | Pit. | 98.89 | 98.46 | 98.46 | 98.46 | 99.13 | 99.13 | 97.60 |
| VGG19 + Bi-GRU | Gli. | 96.11 | 94.08 | 97.71 | 95.5 | 95.56 | 97.79 | 92.85 |
| | Men. | 96.29 | 95.83 | 90.20 | 92.93 | 98.71 | 96.80 | 90.76 |
| | Pit. | 98.54 | 97.66 | 97.69 | 97.69 | 98.92 | 98.93 | 96.62 |

We were able to correctly identify gliomas, meningiomas, and pituitary tumours using our VGG19 + CNN model in every example (see Figure 7a), despite the model's inherent limitations. We classified brain cancers in MRIs using a mix of CNN and RNN models. Combining VGG19 and GRU models allowed for the processing of picture characteristics and the successful learning of brain tumour structural properties.

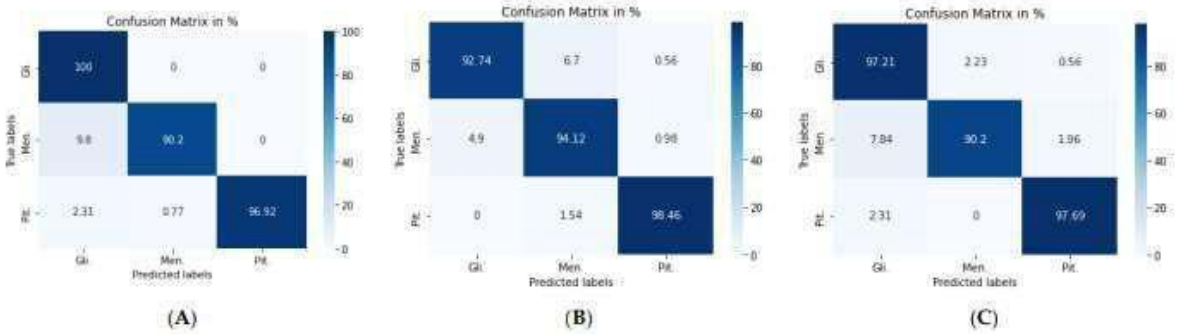


(A) (B) (C)

**Figure 7.** Confusion matrix for: (**A**) VGG19 + CNN model, (**B**) VGG19 + GRU model, and (**C**) VGG19 + Bi-GRU model.

Figure 7. Confusion matrix for: (A) VGG19 + CNN model, (B) VGG19 + GRU model, and (C) VGG19 + Bi-GRU model. The second model (VGG19 + GRU) combined the VGG19 as a feature extractor with GRU as a classifier. The highest accuracy of 94.89% was achieved with the Adam optimizer, as seen in Table 5, with the highest accuracy metric remaining that of pituitary tumors. Figure 7b shows the VGG19 + GRU model confusion matrix, indicating that the model successfully and accurately predicated gliomas, meningiomas, and pituitary tumors at rates of 92.74, 94.12, and 98.46%, respectively. For the third model (VGG19 + Bi-GRU), we used Bidirectional-GRU combined with VGG19 as a classifier of brain tumors. Table 5 shows that the VGG19 + Bi-GRU combination yielded promising results, reaching an accuracy level of 95.62% when coupled with the RMSprop optimizer. The best metrics for accuracy, precision, F1-score, specificity, and MCC were achieved in relation to the identification of pituitary tumors, while sensitivity and NPV were highest in relation to the detection of gliomas. The VGG19 + Bi-GRU model‟s confusion matrix indicated successful prediction rates of 97.21, 90.20, and 97.69% of gliomas, meningiomas, and pituitary tumors, respectively. Figure 7c shows the VGG19 + Bi-GRU model confusion matrix. The losses of the three models during the entire training for the test and validation process versus epochs for the three best models is shown in Figure 8. Figure

7. Confusion matrix for: (A) VGG19 + CNN model, (B) VGG19 + GRU model, and (C) VGG19 + Bi-GRU model. The second model (VGG19 + GRU) combined the VGG19 as a feature extractor with GRU as a classifier. The highest accuracy of 94.89% was achieved with the Adam optimizer, as seen in Table 5, with the highest accuracy metric remaining that of pituitary tumors. Figure 7b shows the VGG19 + GRU model confusion matrix, indicating that the model successfully and accurately predicated gliomas, meningiomas, and pituitary tumors at rates of 92.74, 94.12, and 98.46%, respectively. For the third model (VGG19 + Bi-GRU), we used Bidirectional-GRU combined with VGG19 as a classifier of brain tumors. Table 5 shows that the VGG19 + Bi-GRU combination yielded promising results, reaching an accuracy level of 95.62% when coupled with the RMSprop optimizer. The best metrics for accuracy, precision, F1-score, specificity, and MCC were achieved in relation to the identification of pituitary tumors, while sensitivity and NPV were highest in relation to the detection of gliomas. The VGG19 + Bi-GRU model‟s confusion matrix indicated successful prediction rates of 97.21, 90.20, and 97.69% of gliomas, meningiomas, and pituitary tumors, respectively. Figure 7c shows the VGG19 + Bi-GRU model confusion matrix. The losses of the three models during the entire training for the test and validation process versus epochs for the three best models is shown in Figure 8

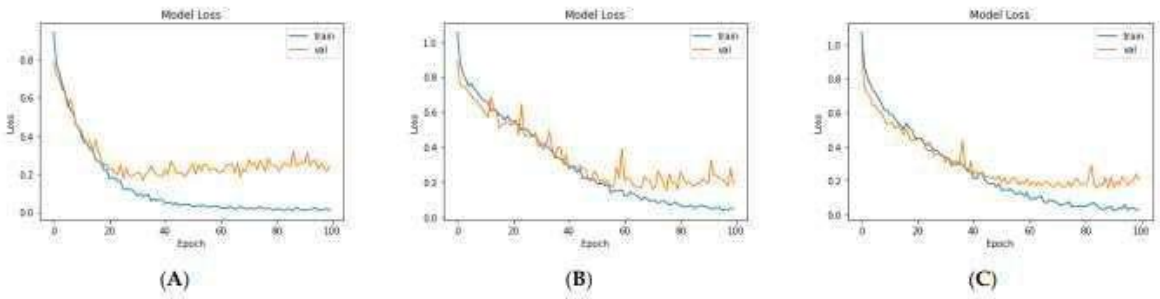


**Figure 8.** Loss over the training process for: (**A**) VGG19, (**B**) VGG19 + GRU, and (**C**) VGG19 + Bi-GRU.

3.3 *Scenario II: Deep Learning Models with PGGAN-BasedDA*

Increasing the model's capacity to categorise brain tumours naturally makes our approach more trustworthy and practically useful. As a result, the experiment's second step included creating synthetic MR images of brain tumours using the PGGAN model in order to make categorization more realistic. PGGAN models were employed in nine different ways: three models for each tumour kind, and one for each plane of the aircraft. An expert radiologist has validated the synthetic MRIs. With the help of an expert radiologist, the results of PGGAN were checked for accuracy and mirrored actual tumour pictures. It was the radiologist's job to make sure that the produced pictures accurately depicted each of the three target tumour types and to detect any 'wrong' photos, which were then thrown out. A "realistic" MR picture is

shown in Figure 9; a “wrong” MR image is shown in Figure 10. MRI brain tumour images created using the PGGAN model were included into the original training data set, and the models' performance was assessed after each was retrained.

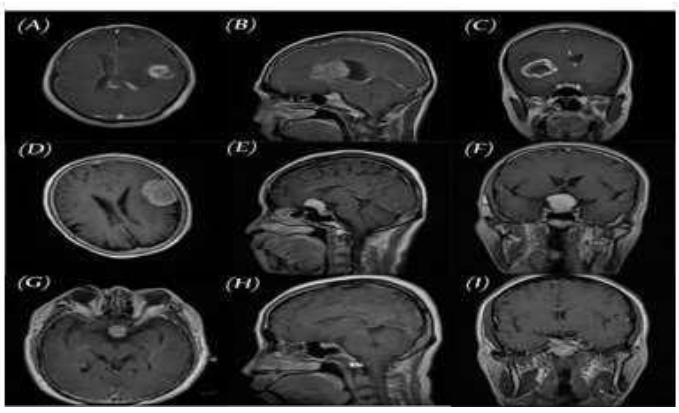


**Figure 9.** Samples of „realistic“ synthetic MR images, in three planes, produced by PGGAN: (**A**– **C**) glioma (**D**–**F**) meningioma, and (**G**–**I**) pituitary tumor.

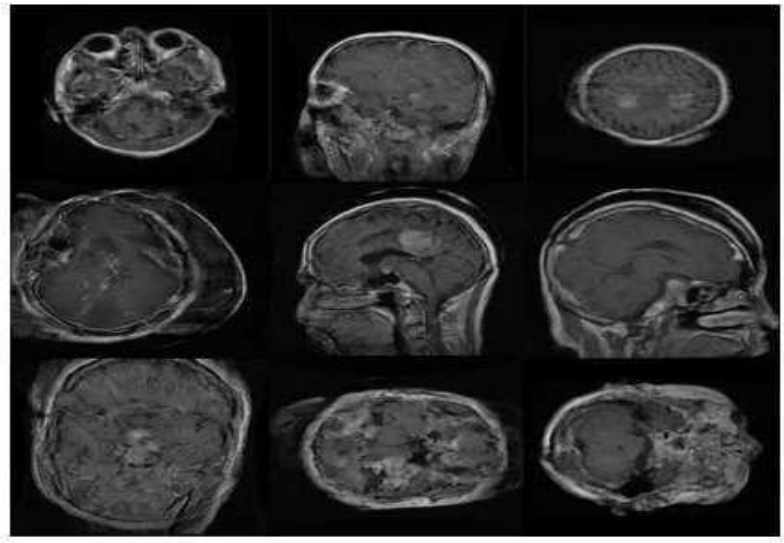

**Figure 10.** Samples of „wrong“ synthetic MR images produced by PGGAN.

## 4. Conclusion

The recent research work in tumor classification based on MR images has witnessed some challenges, such as the number of images in the data set, and the low accuracy of the designed models. This work proposed a complete framework based on a deep learning model as feature extractors with different classifier models designed to classify MRIs of gliomas, meningiomas, and pituitary tumors using different types of augmentations. The feature extractor VGG19 was used to extract features of brain tumor MRIs. Three types of classifiers were then tested (CNN, and the recursive neural networks GRU and Bi-GRU). In our work, the number of images in the data set was increased by using different methods for image augmentation: PGGAN and classic augmentation methods such as rotation, mirror, and flipping. The proposed models achieved more accuracy than the recent introduced models. The CNN classifier yielded the best accuracy performance (98.54%). The VGG19 + CNN model and PGGAN augmentation framework outperformed the other models in all previous work, with accuracy values of 98.54, 98.54, and 100% for gliomas, meningiomas, and pituitary tumors, respectively.